POLITECNICO DI TORINO

Master's Degree Program in Aerospace Engineering

IMPERIAL

Master's Degree Thesis

Numerical Modelling of Wave Propagation in Granular Crystals for Aero-Engine Applications

Supervisors

Prof. Daniele BOTTO

Dr. Alfredo FANTETTI

Candidate

Samuele FERRERO

December 2024

Summary

The aviation sector is at a pivotal point, facing the need to develop environmentally sustainable and efficient engines while remaining lightweight. A critical factor to consider during the design phase is the dynamic response of the engine, which, given its construction from millions of components, presents challenges in correlating experimental friction data with computational models. This Master Thesis aims to overcome some of these challenges by using wave propagation to improve the understanding of friction. Specifically, a numerical model in MATLAB that simulates the propagation of solitary waves in granular crystals, incorporating frictional effects, is developed. Like traditional ultrasonic waves, solitary waves are used as tools for non-destructive evaluation. However, the innovation presented here lies in using solitary waves to monitor friction, as unlike ultrasonic waves, they have not been applied to this purpose before. After an initial section on the state of the art and relevant literature, the project progresses to the development of a MATLAB computational model for simulating the propagation of solitary waves through a chain of granular crystals (modeled via Discrete Element Method, DEM) and a metal block (modeled via Finite Element Method, FEM). This setup will enable a series of physical insights by observing how friction alters the system. Once validated, the model may be applied to analyze components affected by friction, such as turbine-bladed disks with friction dampers. This project's ultimate goal is to first correlate changes in solitary wave propagation through a medium with the friction properties of sliding contacts, thereby developing a novel tool that could drive significant advancements in tribology and dynamics.

A nonna Carmen e nonno Francesco,
il vostro terremoto

Acknowledgements

The most important thanks go to my mom, dad, and Francesca for always helping and supporting me unconditionally, in happy moments and especially during difficult times. Thank you.

I would like to thank Dr. Alfredo Fantetti, my supervisor at Imperial College London, for guiding me and teaching me patiently about new and innovative topics.

I would also like to thank Prof. Daniele Botto, my supervisor at the Politecnico di Torino, for helping me to get in touch with this engineering field.

I would like to thank all my friends, who have always been by my side, and everyone who has supported me throughout these years at university.

Table of Contents

List of Tables

List of Figures

Acronyms

SW
Solitary wave

GC
Granular crystal

DEM
Discrete element method

FEM
Finite element method

DOF
Degree of freedom

FE
Finite element

ODE
Ordinary differential equation

Chapter 1

Introduction and literature review

1.1 Motivations and experimental setup

Granular crystals are an artificial material composed of particles in contact with one another. They can be classified based on how the constituent particles are arranged within the material, allowing for the distinction of one-dimensional (1D), two-dimensional (2D), or three-dimensional (3D) granular crystals. The uniqueness of this type of material lies in its ability to study problems in nonlinear dynamics. Nonlinearity in granular crystals arises from the Hertzian interaction that occurs between adjacent particles [1].

The simplest way to create a 1D granular crystal is by arranging a chain of spherical particles in contact with one another. Experimentally, nonlinear waves can be generated through the impact of a striker, a vibrational exciter, or a piezoelectric transducer. The nonlinear wave generated as a result of one of these stimuli is a solitary wave. This type of wave can be used similarly to traditional ultrasonic waves to better understand friction in components of interest, both in aeronautical applications and beyond.

The experimental and computational setup of this work involves a chain of spherical particles (granular crystal) in contact (considering friction) with a half-space wall, which is subjected to a sinusoidal displacement. This setup allows for the investigation of the behavior and relationship between friction and solitary wave propagation, with the goal of developing a device for friction monitoring. Such a device could be applied to components for which experimental campaigns are challenging, thereby leveraging the potential of computational simulation.

1.2 Thesis outline

In the following section the structure of the thesis is presented: In the following section, the structure of the thesis is presented:

- Chapter 1: A brief introduction to the problem followed by a review of solitary waves in granular crystals and their relation to friction.
- Chapter 2: The model and simulations related to the granular crystal composed of N particles are presented, focusing on the initial impact generating the formation of a solitary wave.
- Chapter 3: The model and simulations aimed at characterizing the metal block, representing the component under investigation for solitary wave propagation, are introduced.
- Chapter 4: The coupling mechanism of the two models is described, enabling a comprehensive simulation.
- Chapter 5: The influence of friction is analyzed.
- Chapter 6: The conclusions of the thesis are presented, along with possible future directions in this field of study.

1.3 Solitary waves in granular crystal

Granular crystals (GCs) are a type of artificial material composed of particles (macroscopic or microscopic) in contact with each other. The term "crystal" is used to distinguish these synthetic materials from natural granular materials such as soil. As mentioned in 1.1, the uniqueness of these materials lies in their ability to facilitate the generation and propagation of solitary waves, making them highly interesting for the study of problems in nonlinear dynamics. This phenomenon was demonstrated through the studies of Nesterenko, who theoretically [2] and experimentally [3] proved the emergence of solitary waves in granular crystals. The solitary wave within a granular crystal, which can be constructed as a chain of spherical particles in contact with one another, arises and propagates according to Hertzian laws [4].

1.3.1 Hertzian laws

For Hertz's laws to be considered valid, certain assumptions must be made:

- The deformation of the particles in contact must remain within the elastic limit.

- The contact surface between the two particles must be much smaller than the diameter of each particle.
- The wave frequency of the granular crystal must be much lower than the oscillation frequency of each individual particle.
- Friction between particles is considered negligible.

The Hertzian contact law states that the force between two particles in contact can be defined as follows [1]:

$$F_{i,i+1} = A_{i,i+1}[\delta_{i,i+1}]_+^{p_{i,i+1}} \tag{1.1}$$

where i and $i+1$ represent the indices of the two adjacent particles, A is a coefficient that depends on the mechanical and geometric properties of the adjacent particles, the exponent p varies according to the shape of the particles in contact [5], and δ is the relative displacement between the two particles. In the case of interest, the exponent $p = \frac{3}{2}$ because the particles involved are spherical in shape. The exponent p makes the force between two particles in Hertzian contact a nonlinear force.

Moreover, $[\cdot]_+$ indicates that the relative displacement equals itself when it is greater than zero, meaning the particles are in actual contact, and it assumes a value of zero otherwise. Thus, the Hertzian force arises only when there is contact between the two particles, which is another factor contributing to the nonlinearity of a granular crystal.

1.3.2 State-of-the-art solitary waves

Solitary waves within granular crystals have been extensively studied and analyzed in recent years. A study by Yang et al. [6] revealed that, when evaluating the interaction between highly nonlinear solitary waves and thin large plates, the reflected solitary wave exhibits delay and attenuation strongly influenced by the boundary conditions of the plate. Specifically, these effects are attributed to the inelasticity inherent to large plates, caused by the dispersion of elastic waves within the plate. Additionally, the coupling behavior between the granular chain and the plate is shown to depend on the boundary conditions within a certain critical distance. This study further highlights the importance and potential of a 1D granular crystal as a nondestructive evaluation tool for assessing the mechanical properties of plate structures. Unlike conventional ultrasound techniques typically used for this purpose, the granular crystal offers greater portability and energy efficiency, making it an ideal candidate for nondestructive evaluation applications.

The study conducted by Carretero-Gonzàlez et Al. [7] presents a systematic model for dissipation in granular crystals, incorporating a phenomenological term based on the velocity difference between adjacent beads (a discrete Laplacian)

raised to a common exponent. This augmentation of the standard Hertzian-based dynamical model successfully captures dissipation effects, achieving optimal agreement with experimental results across various materials, including steel, Teflon, and brass. The dissipation prefactor was found to be material-dependent, with Teflon exhibiting a significantly weaker prefactor compared to brass and steel. This allowed the unambiguous observation of secondary waves for the first time. Future directions include investigating the critical prefactor threshold for secondary wave emergence, the interplay between dissipation and plasticity, and extending the model to higher-dimensional systems.

The article presented by Jalali et Al. [8] presents a numerical study on a nondestructive evaluation (NDE) method based on the propagation and detection of solitary waves, focusing on detecting localized corrosion in steel structures. The results show that the method is more sensitive to corrosion in thinner plates and that its sensitivity improves with larger, heavier, and stiffer particles. The length of the granular chain and the position of the sensor particle have minimal impact on the reflected solitary waves. However, in high-temperature environments, longer chains and distancing the sensor from the object help protect sensitive PZT wafers. Additionally, using silicon nitride particles is advantageous due to their stiffness and low thermal conductivity, offering protection in hot zones.

Another study conducted by Santibanez et Al. [9] experimentally investigates the interaction between two solitary waves in a linear chain of spheres interacting via the Hertz potential. When counterpropagating waves collide, they pass through each other, introducing a phase shift due to the nonlinear interaction potential. Numerical simulations accurately reproduce this behavior, showing that it is independent of viscoelastic dissipation at bead contacts. For collisions of equal amplitude, synchronized waves, two secondary solitary waves emerge from the interaction region. The amplitude of these secondary waves is proportional to the incident wave amplitude but is stronger when the collision occurs at the middle contact of chains with an even number of beads. While numerical simulations predict the existence of secondary waves, experiments reveal significantly larger amplitudes than expected, attributed to rolling friction at bead contacts during wave propagation.

1.4 Hysteresis Loop and Friction

The hysteresis loop is obtained by plotting the friction force against the relative displacement generated between two oscillating surfaces in contact. From this plot, it is possible to derive fundamental quantities such as the tangential contact stiffness, the friction coefficient, and the dissipated energy (the area of the loop). Figure 1.1 shows a typical hysteresis loop measured using a friction rig [10] developed at

Imperial College London and Politecnico di Torino. The following contact states can be observed:

- $0 \rightarrow 1$: Initial loading
- $1 \rightarrow 2$, $4 \rightarrow 5$: Sticking regime
  Since the tangential contact force is linearly related to the relative displacement, the tangential contact stiffness is simply calculated from the slope of the curve. This quantity can strongly influence the resonance frequencies of the system.
- $2 \rightarrow 3$, $5 \rightarrow 6$: Microslip
  This occurs between the sticking regime and the gross slip regime and is characterized by partial slip in some areas while other portions remain stuck.
- $3 \rightarrow 4$, $6 \rightarrow 1$: Gross slip
  The entire contact surface is in full relative sliding motion. In this contact state, the friction force is approximately constant and equal to the friction limit μN. During this phase, energy is dissipated, which is an important parameter for nonlinear dynamic analysis.
- Separation
  This phase, not shown in Figure 1.1, occurs when the normal load becomes zero, and no tangential contact force is transmitted.

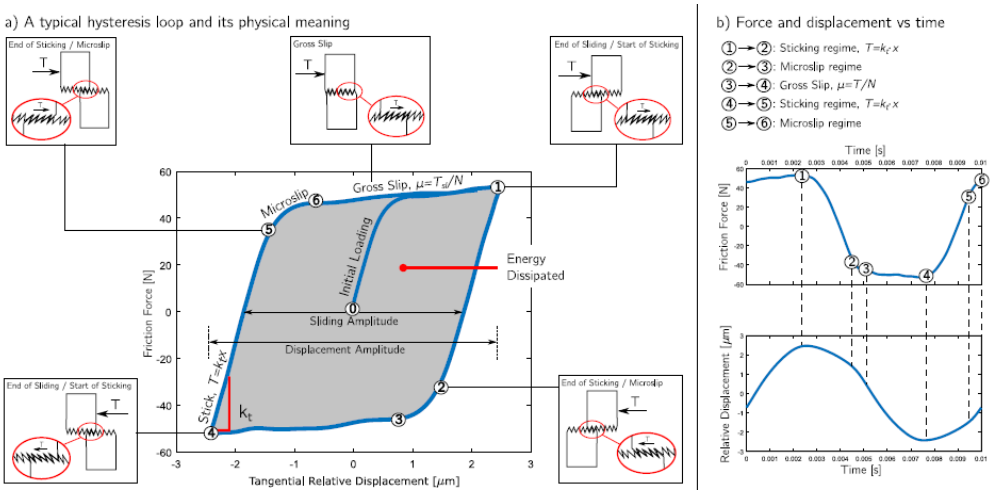

Figure 1.1: A typical hysteresis loop [10]

The friction force is the resistance to the relative motion between surfaces or substances moving past one another or attempting to move tangentially relative to

each other. It is generally quantified as a force or as a dimensionless parameter, such as the friction coefficient [11].

The first studies on friction were conducted in the 15th century by Leonardo da Vinci [12], who observed that the friction force was proportional to the applied normal load and independent of the nominal contact area. Subsequently, Bowden and Tabor [13] made significant progress in understanding friction by demonstrating that the tangential force required to slide a contact junction is proportional to the junction area through a critical shear strength. This implies a linear relationship between the friction force and the real contact area, explaining the origin of the empirical friction law, provided there is proportionality between the real contact area and the normal load. Howell [14] later generalized the friction laws, which are typically described as follows:

- $F = \mu R$, where F is the limiting frictional force, and R is the normal reaction.
- The friction coefficient μ is independent of the apparent contact area.

These laws can be generalized by considering a law of the form:

$$F = aR^n \tag{1.2}$$

where n varies depending on the material considered, particularly ranging between 0.67 and 1 for metals.

Considering Equation 1.2, the following observations can be made:

- Amonton's law $F = \mu R$ is a special case of 1.2 where $n = 1$.
- F now depends on the apparent area and is independent only when $n = 1$.
- If roughening a surface creates valleys significantly larger than the spacing between surface asperities, the available area for real contact decreases, leading to a corresponding reduction in frictional force.
- The coefficient a is dimensional, except when $n = 1$.

1.5 Contact model

The previously mentioned models by Da Vinci, Amontons, and Coulomb are classified as classical or quasi-static friction models. Another type of model is the dynamic friction model, which considers friction as a velocity-dependent function and introduces time-varying variables. Additionally, there is another class of models known as hysteretic friction models, which originate from elasticity theory to describe energy dissipation and deformation.[15]

1.5.1 Quasi-Static Friction Models

The most well-known and widely used models are the Coulomb friction model [16], characterized by a velocity-independent friction coefficient, and the viscous friction model [17], which assumes a linear relationship between the friction force and the relative velocity. By placing an elastic spring in series with a Coulomb element, the Jenkins element [18] is obtained. This element is employed in Section 5 to plot hysteresis curves.

1.5.2 Dynamic Friction Models

Dynamic models were developed to address issues in control engineering, where accounting for friction is critical for control design. Examples of such models include the Dahl model [19], which represents a stress-strain curve using a differential equation, and the LuGre model [20], which extended the Dahl model by incorporating the Stribeck effect [21]. Further advancements were achieved with the Leuven model [22].

1.5.3 Hysteretic Friction Models

The reference model for this class is the Masing model [23], which considers effects arising from plastic and elastic deformation. It is composed of Jenkins elements arranged in parallel with a spring. The strength of this model lies in its generalizability, as it can be extended to a system consisting of several springs in series with Coulomb elements. This configuration is known as the Iwan model [24].

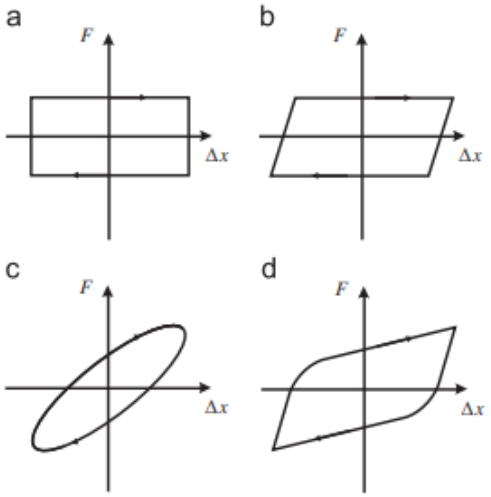

Figure 1.2: a) Coulomb model, b) Jenkins model, c) constant hysteresis model, d) various dynamic/hysteresis models

Chapter 2

Model for the granular crystal

2.1 Numerical modeling

The interaction between particles is described by the well-known Hertzian interaction law, according to which the force is proportional to a $\delta^{\frac{3}{2}}$, where δ represents the relative displacement between two contiguous particles. In a system composed of N particles, the equation of motion for the n-th particle is described by [6]:

$$m\ddot{u}_n = A_n[u_{n-1} - u_n]_+^{3/2} - A_{n+1}[u_n - u_{n+1}]_+^{3/2} + mg, \quad n \in \{1, \dots, N\} \tag{2.1}$$

$$A_n = \begin{cases} A_s = \frac{E_s\sqrt{D}}{3(1-\nu_s^2)}, & n \in \{1, \dots, N\} \\ A_p = \frac{2}{3}\sqrt{2D}\left(\frac{1-\nu_s^2}{E_s} + \frac{1-\nu_p^2}{E_p}\right)^{-1}, & \text{n = N + 1} \end{cases} \tag{2.2}$$

where m represents the mass of the $n-th$ particle, and u_n is the displacement of the $n-th$ particle from its rest position (without applied load). It is important to note that the contact force will only arise for a positive displacement δ, indicating that penetration has occurred between the two particles. In fact, in the absence of contact and thus penetration, a contact force can't be generated. The governing equation for the motion of the $n-th$ particle expresses the 2^{nd} law of dynamics, relating the inertial force $m \cdot a$ to the contact force generated by the penetration between particles in the granular chain. From a numerical perspective, the solitary wave propagating within the granular crystal is modeled using a discrete element method (DEM). For propagation within the plate, however, a spectral element method (SEM) should be used, which represents an advanced form of the finite element model designed to minimize numerical errors and computational costs. Focusing on wave propagation within the chain of granular crystals, it becomes evident that a system of ordinary differential equations (ODEs) must be solved. Considering a

chain of N particles, this results in a system of N differential equations. Defining u as the vector consisting of the displacements of the N particles

$$U = \begin{bmatrix} u_1 \\ u_2 \\ \vdots \\ u_N \end{bmatrix} \tag{2.3}$$

and $f(u)$ as the right-hand side of the differential equation, the solution can be formulated as $u'' = f(u)$. Dealing with a second-order equation requires transforming it into a system of first-order equations, given by

$$\dot{z} = F(z) = \begin{bmatrix} \dot{U} \\ f(U) \end{bmatrix} \tag{2.4}$$

where $\dot{U}$ is the time derivative of U and is equal to

$$\dot{U} = V = \begin{bmatrix} v_1 \\ v_2 \\ \vdots \\ v_N \end{bmatrix} \tag{2.5}$$

This is the equation that will be solved using a MATLAB script. Solving this equation yields both the velocity and displacement for each particle in the granular crystal chain. With velocity and displacement data available, physical and/or numerical considerations can then be made, which will be presented in the following section.

The initial conditions for the problem are: zero initial velocities for all particles except the first particle, which will have an initial velocity such that it acts as the *striker* in the system, initiating the formation of the solitary wave; initial displacements are zero throughout, meaning that the N spheres are spaced $2R$ apart, in contact but without mutual penetration. Physical parameters such as the radius, number of particles, elastic moduli, Poisson's ratios, and densities of both the spheres and the plate, along with particle masses, are provided. These parameters allow the calculation of coefficients A_n and thus facilitate writing the differential equation.

Using a solver implemented in MATLAB (e.g., 'ode45' [25]), the system of differential equations can be solved. Since in this initial phase only the propagation of the solitary wave in the granular particle chain is being considered, further iterations in the code are not necessary.

In Figure 2.1, a schematic representation of the system is shown: N spheres representing the granular crystal are interconnected, with the last sphere colliding

against a wall ideally assumed to have infinite stiffness. Initially, the wall serves as a schematic representation of the FEM block, which will be introduced in Chapter 3.

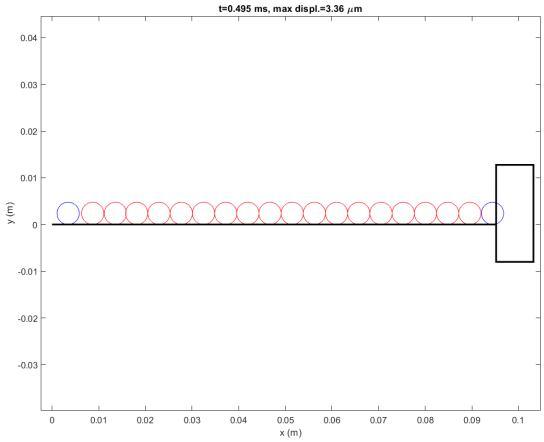

Figure 2.1: Schematic representation of the system

2.2 Physical considerations

2.2.1 Displacement and velocities

By plotting displacement and velocity as a function of time, it is possible to observe the interactions between the various particles. In the displacement-time graph, we can see that initially the first particle moves in the positive x-direction, penetrates a micrometric amount into the second particle, and then at a certain point moves backward (showing negative displacement values). In the velocity-time graph, we observe the propagation of the solitary wave. Specifically, if we examine the moment when the motion begins (when the second particle has a non-zero velocity), we can calculate the wave propagation speed as the distance traveled divided by the measured time. At a certain instant (0.18 ms), an inversion of the velocity sign of all N particles is observed. This can be attributed to the impact of the last particle with the plate, which generates a reflection of the solitary wave.

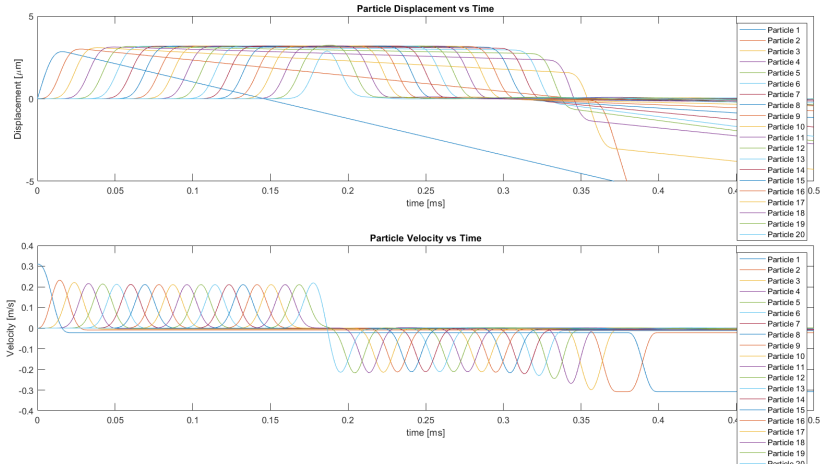

Figure 2.2: Displacement and velocities

2.2.2 Velocity of the solitary wave

Another important quantity to calculate is the velocity of the solitary wave.

2.2.3 Contact and inertial forces

It is possible to represent the inertial and contact forces acting on the n-th particle to verify the validity of the second law of dynamics applied to the n-th particle, according to which the inertial force must equal the sum of the forces acting on it.

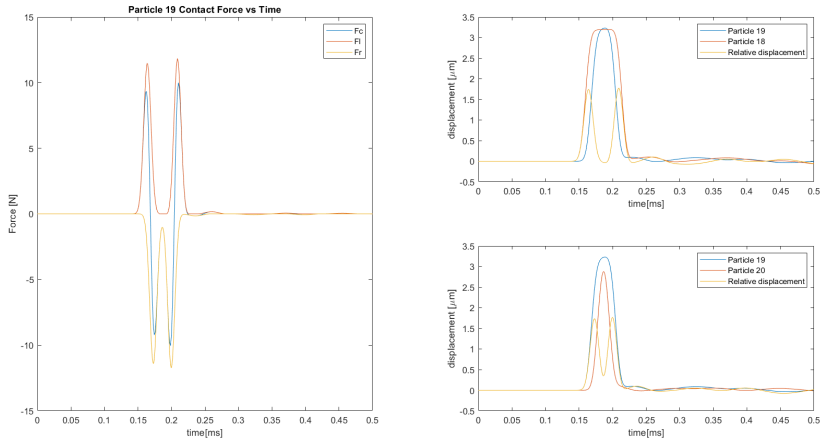

Figure 2.3: Contact force for the 19th particle

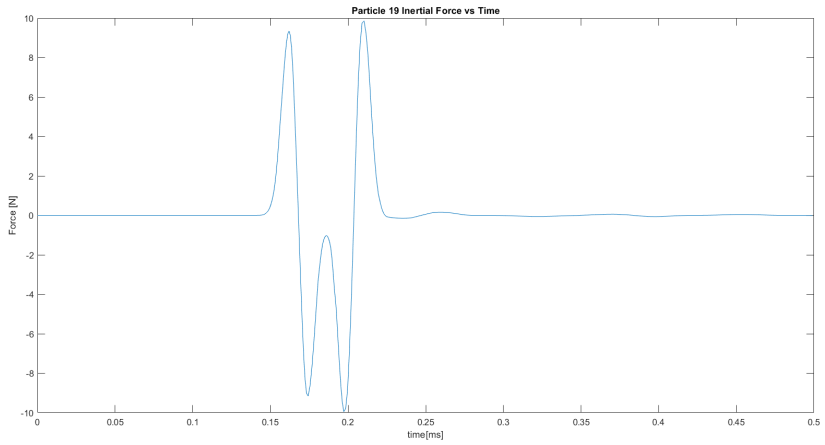

Figure 2.4: Inertial force for the 19th particle

2.2.4 Energy

The time evolution of the energy within the system can be evaluated [26]. Since there is no dissipation in this initial phase of the analysis, a constant trend of the system's mechanical energy (given by the sum of the mechanical energy of each particle) is expected. This is obtained from the sum of kinetic and potential energy. At the initial moment, the particles are in contact, but there is no penetration, so the potential energy is zero, while there is a certain amount of kinetic energy due to the initial motion of particle 1. The motion proceeds as the first particle penetrates into the second, generating a component of potential energy and a corresponding decrease in kinetic energy. The motion continues with the penetration of the second particle into the third, and so on. The trend of the system's total energy can be observed to remain constant over time (aside from purely numerical errors).

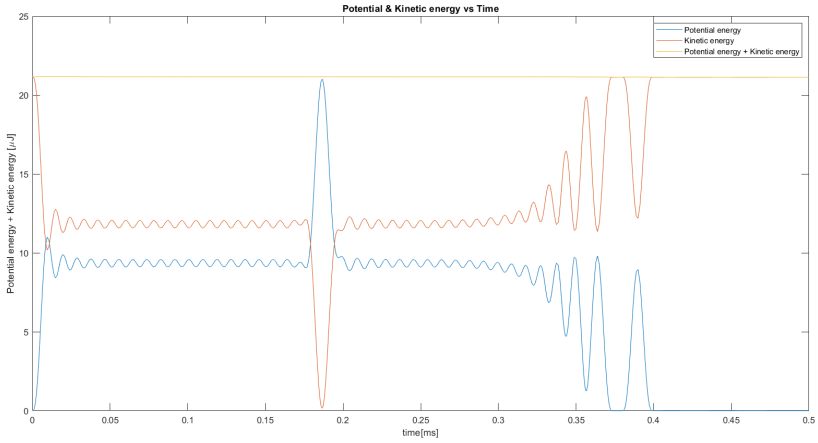

Figure 2.5: Energy of the system

2.2.5 Sensitivity Analysis

This section analyzes the effects of changing certain physical parameters (effects of varying exponent, initial velocity, stiffness, mass, radius).
Exponent: The exponent in the Hertzian formulation $\frac{3}{2}$ allows for a constant coefficient A_j independent of the applied load, depending only on geometric parameters. This way, the contact force can be expressed as $F = A_j\,\delta x^{3/2}$. If we were to use the "standard" formulation $F = kx$, the dependency of k (contact stiffness) on the applied load would need to be considered.

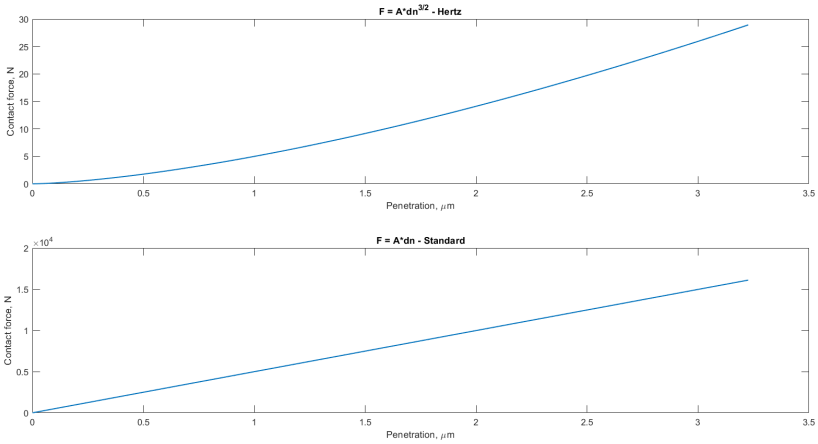

Figure 2.6: Normal load vs penetration

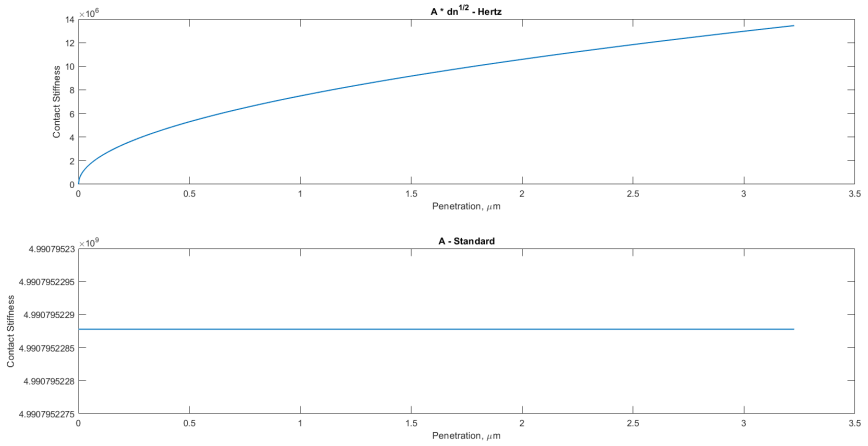

Figure 2.7: Contact stiffness vs penetration

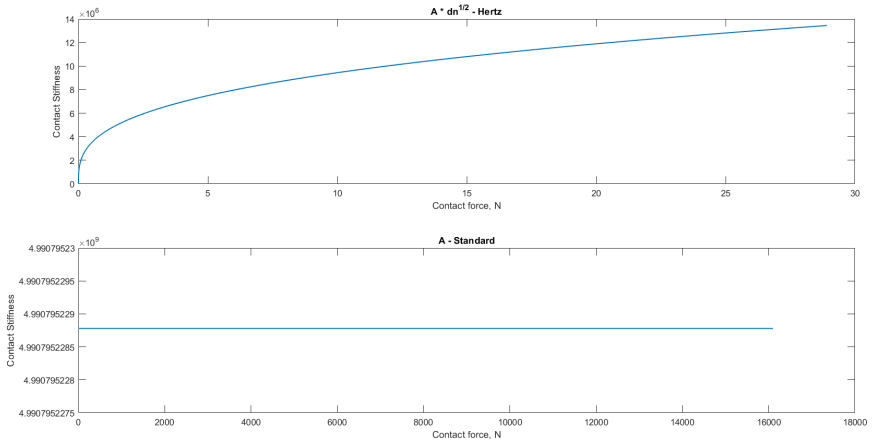

Figure 2.8: Contact stiffness vs normal load

It is observed that the solitary wave propagation speed does not depend on the initial velocity when using the formulation $F = kx$, but there is a strong dependence when using the 3/2 exponent formulation. Physically, using an exponent value of 1 transforms the system of N spheres into a continuous single-bar system. In this case, the propagation speed corresponds to the speed of sound in this material. Indeed, the speed of sound in a metal represents the phase between consecutive particles. It is essential to distinguish between the wave propagation speed and the individual particle velocity in the granular chain (these are two completely different quantities). A smaller phase ϕ indicates particle movement in unison

($\phi = 0$ ideally for a perfectly rigid body), whereas a value greater than zero for ϕ indicates some elasticity in the contact between particles, with a certain "delay" in penetration between two particles and consequent signal propagation (solitary wave). The exponent varies and is different for each body under consideration: for a bar, it is equal to 1, since the material is homogeneous; in a sphere, the contact area increases as contact increases, resulting in a 3/2 exponent (greater than 1).

Stiffness: Stiffness represents the rigidity of the contact established between consecutive particles. An increase in stiffness leads to a higher wave propagation speed, as the "delay" time for the previous particle to penetrate the next is reduced, thus accelerating the solitary wave's travel.

Radius: The influence of the radius does not come into play, as in a DEM model, each sphere is treated as a material point with a certain mass. While the mass depends on the radius, it does not affect the equations, as the mass acts as a common divisor across the system.

Radius mm	Speed of propagating front $\frac{m}{s}$
10	365
30	365
100	365

Table 2.1: Dependence of the propagation velocity on the sphere radius

Initial velocity:

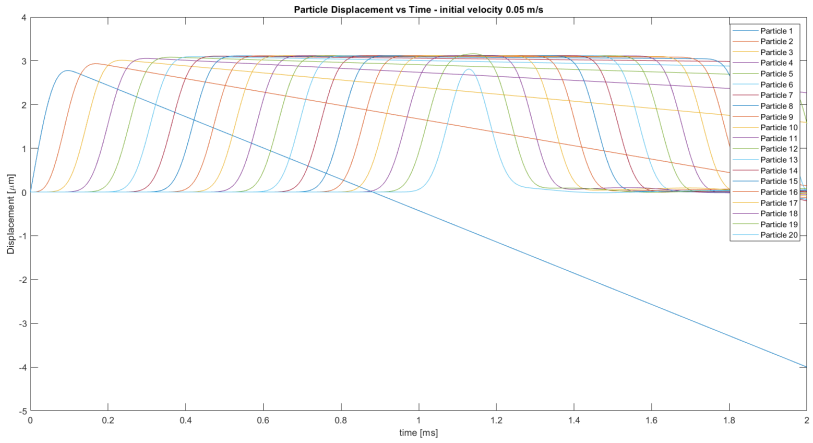

Figure 2.9: Initial velocity 0.05 $\frac{m}{s}$

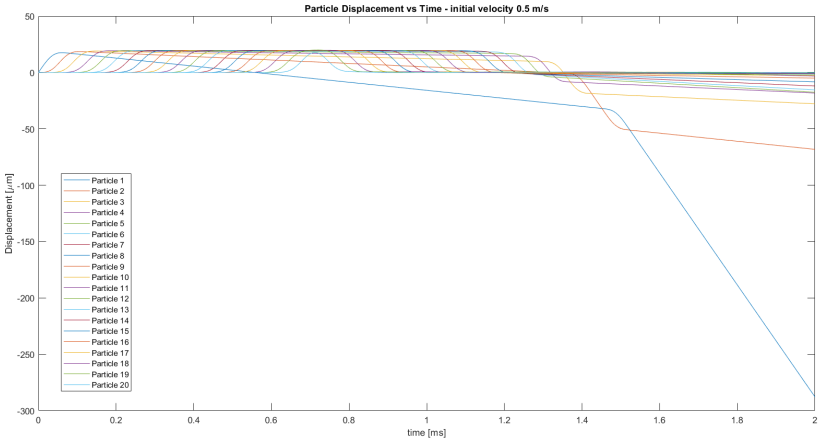

Figure 2.10: Initial velocity 0.5 $\frac{m}{s}$

Initial velocity $\frac{m}{s}$	Speed of propagating front $\frac{m}{s}$
0.5	578
0.05	365

Table 2.2: Dependence of the propagation velocity on the initial velocity of the striker

Steady state: It would be possible to evaluate the existence of a steady state by introducing a wall before the first particle. Using an autocorrelation algorithm, a cyclic signal related to the individual particles could be sought.

2.2.6 Other quantities

Other quantities that can be evaluated are as follows:

- The maximum particle velocity attained during the solitary wave propagation [27]:

$$v = 0.682 \cdot v_0 \tag{2.6}$$

  where v_0 is the impulse velocity of the striker particle.

- The analytical contact time for the last particle of the chain on a semi-infinite wall (which is our case) [6]:

$$T_c = m^{\frac{2}{5}} \cdot v^{-\frac{1}{5}} \cdot A_p^{-\frac{2}{5}} \tau_c \tag{2.7}$$

where A_p is given by 2.2 [28], v is the maximum particle velocity, and τ_c is the dimensionless contact time, approximately equal to 3.22 for a semi-infinite wall [29].

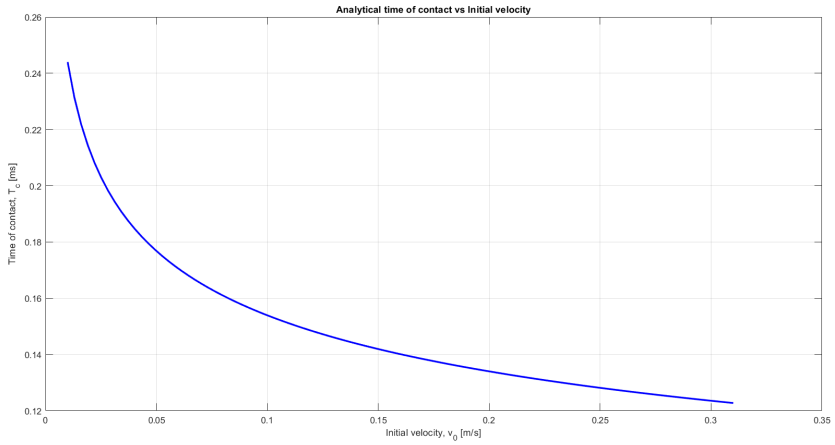

Figure 2.11: Analytical time of contact

- The analytical solitary wave speed in an **uncompressed** 1D monodisperse chain [6]:

$$V_s = 0.64^{1/5} \left(\frac{2E_s}{\rho_s \pi} \right)^{2/5} v_{\text{in}}^{1/5} \tag{2.8}$$

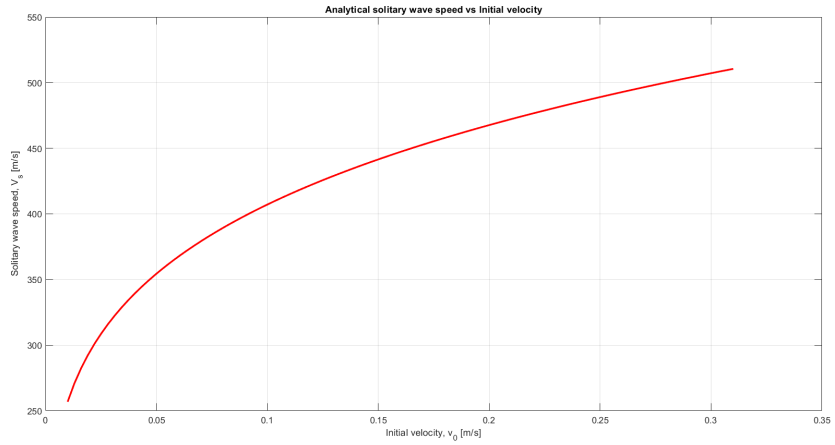

Figure 2.12: Analytical solitary wave speed

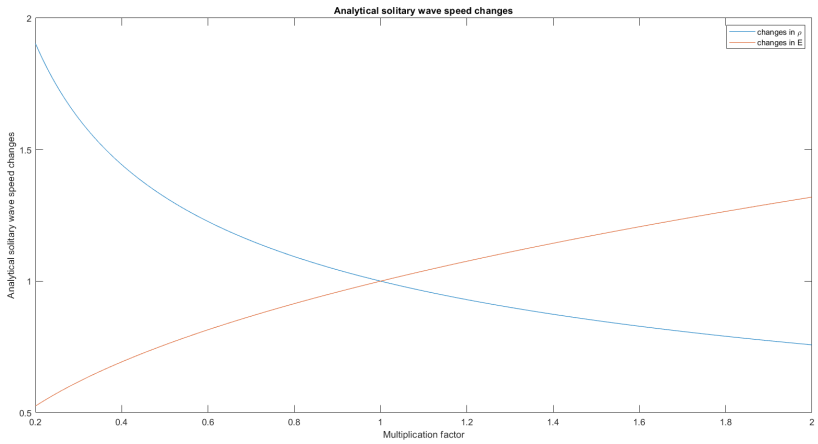

Figure 2.13: Analytical solitary wave speed dependency

In figure 2.13, the behavior of the analytical solitary wave (see 2.2.6 for the formulation) is shown as a function of E and ρ. The graph is intended as a qualitative representation only.

2.3 Dissipation

In Section 2.1, a non-dissipative system was considered, i.e., an ideal system in which the mechanical energy remains conserved over time. However, to consider a more realistic case, it is necessary to include the dissipative effect in Equation 2.1. This dissipation can be evaluated using the restitution coefficient [30]:

$$\epsilon = \left(\frac{U_{n+1}}{U_n}\right)^{1/2} = \left(\frac{F_{n+1}}{F_n}\right)^{5/6} \tag{2.9}$$

where U_n is the Hertz potential, i.e., the work done by the Hertz force F_n at the contact n. The dissipation mechanism arises from two primary processes:

- Internal viscoelasticity
- Solid friction of beads under their weight
- Solid friction between beads due to hindered rotations (this is not considered here)

For a dissipative system, Equation 2.1 becomes [7]:

$$m\ddot{u}_n = A_n[u_{n-1} - u_n]_+^{3/2} - A_{n+1}[u_n - u_{n+1}]_+^{3/2} + mg + \gamma s\|\dot{\delta}_n - \dot{\delta}_{n+1}\|^{\alpha} \tag{2.10}$$

where $\delta_n = \max\{u_{n-1} - u_n, 0\}$ for $n \in \{1, \ldots, N\}$, $\delta_1 = 0$, $\delta_{N+1} = \max\{u_n, 0\}$, and $s = \operatorname{sgn}(\delta_n - \dot{\delta}_{n+1})$. The implementation in MATLAB is achievable using the *heaviside* function.

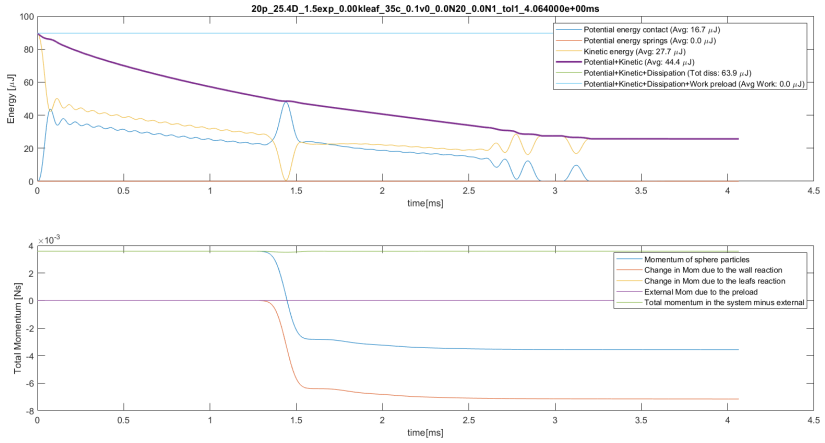

Figure 2.14: Energy and momentum

In Figure 2.14, it can be observed how dissipation reduces the system's mechanical energy. By adding the dissipated energy to the mechanical energy, a constant trend is obtained, indicating the validity of the simulation.

Chapter 3

Model for the block of metal

3.1 Relevance of the block

The metallic block represents the component under investigation for the propagation of solitary waves. This block is made of stainless steel with an elastic modulus of $E = 210\,\text{GPa}$ and a density of $\rho = 8352\,\frac{\text{kg}}{\text{m}^3}$. The block dimensions are $(48.5 \times 56 \times 40)\,\text{mm}$, chosen to ensure that the block can be considered as a half-space wall while also being easily manufacturable for experimental analyses.

3.2 Numerical Modeling

To study the effects and propagation of a solitary wave through this block, it is necessary to solve a structural dynamics problem. This requires solving the following equation:

$$[M]\{\ddot{U}\} + [C]\{\dot{U}\} + [K]\{U\} = \{F(t)\}, \tag{3.1}$$

where F represents the vector of forces and moments applied to the nodes, K is the global stiffness matrix, U is the unknown vector of nodal translations and rotations, C is the damping matrix, and M is the mass matrix of the system. This system can be solved using computational software such as *Abaqus* [31], or analytically via a custom script implemented in *MatLab*.

3.2.1 Abaqus

Abaqus is a finite element method (FEM) simulation software used for advanced engineering analysis. Developed by Dassault Systèmes, it is known for its versatility in solving complex problems across various fields, including structural mechanics, thermal analysis, fluid dynamics, and multi-physics interactions. The use of Abaqus

is crucial not only to obtain the displacements for each degree of freedom of the structure but also to extract the global stiffness matrix K and the mass matrix M. In fact, the mass matrix will be essential for conducting a dynamic analysis, where the load varies over time. To extract the matrices of interest, a frequency analysis is performed. This analysis consists of a series of steps that need to be carried out in order. First, the reference geometry is created, a rectangular prism with the following dimensions:

- height $h = 48.5\,\text{mm}$
- long side $l_1 = 56\,\text{mm}$
- short side $l_2 = 40\,\text{mm}$

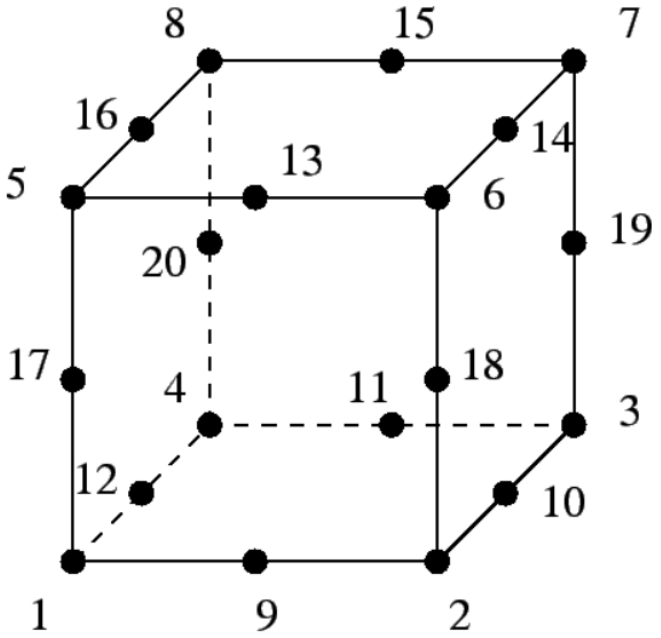

Figure 3.1: CD20R element

Mechanical properties must then be applied to this geometry. Specifically, the elastic modulus and density are assigned as described in 3.1, with a Poisson's ratio $\nu = 0.30$.

The next step is to discretize the structure into parts or finite elements, a process known as *meshing*. This operation must be carried out with certain considerations [32]. First, the individual finite elements must have a shape compatible with their type. Furthermore, the finite elements should not be excessively distorted or contain singularities within them. The chosen element is the **CD20R** (see figure

3.1), a general-purpose quadratic brick element, with reduced integration (2x2x2 integration points). This element is suitable for a wide variety of situations and performs well even for isochoric materials.

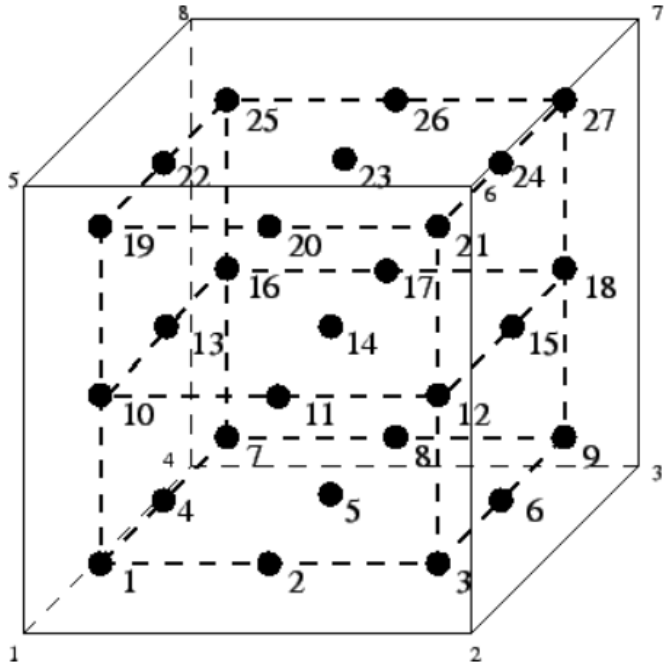

Figure 3.2: CD20R integration scheme

The resulting test mesh is presented in figure 3.3. It can be noted that the elements are of the CD20R type by the fact that each side of the mesh is formed by such elements.

To perform a frequency analysis to extract the matrices to be used in MatLab, boundary conditions must be applied to the block, corresponding to a clamping near the face opposite to the one that will come into contact with the granular crystal. The clamping restricts all degrees of freedom of the nodes in question. The frequency analysis provides the modes and natural frequencies of oscillation of the structure, which are essential for comparing the results obtained in MatLab. To extract the K and M matrices (see in detail A), the appropriate command is inserted into the *.inp* file generated by Abaqus, which is then re-executed from the command window. Abaqus is also useful for understanding which node, and thus the corresponding degree of freedom, will come into contact with the last particle of the granular crystal. To do this, a static analysis is performed, which consists of defining a static load and applying it at the central point of the face opposite the clamped one. Using a procedure similar to the matrix extraction, the load matrix

and the corresponding loaded degree of freedom are extracted. Moreover, from the static analysis, the displacement field of the structure is obtained, which is the essential starting point for the coupling between the DEM and FEM models, as discussed in chapter 4.

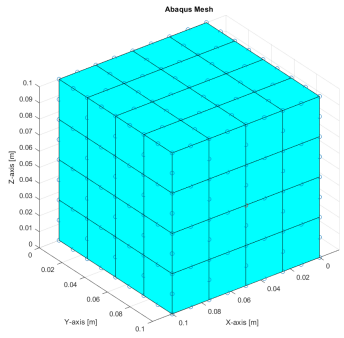

Figure 3.3: Mesh

3.2.2 MatLab

MatLab is used to implement a script that solves the system 3.1. This is done using *ode15s* [33]. It is chosen because it solves stiff differential equations. In particular, it is useful for solving systems of ordinary differential equations (ODEs) that exhibit stiffness, which means they have rapidly changing solution in some regions and slowly changing solutions in others. Indeed, it is expected that the solution will vary more rapidly near the node where the force is applied, while it will vary more slowly at the boundaries of the computational domain.

The mass and stiffness matrices are imported into MatLab and used for this purpose. Some fundamental quantities are defined to solve the problem. We define the vector of displacements and rotations for the degrees of freedom of the structure as

$$U = \begin{bmatrix} u_1 \\ u_2 \\ \vdots \\ u_{dof} \end{bmatrix} \tag{3.2}$$

and the vector of linear and rotational velocities of the degrees of freedom as

$$V = \begin{bmatrix} v_1 \\ v_2 \\ \vdots \\ v_{dof} \end{bmatrix} = \dot{U} \tag{3.3}$$

In this way, the system 3.1 can be expressed as:

$$\{\ddot{U}\} = f(U) = \frac{\{F(t)\} - [C]\{\dot{U}\} - [K]\{U\}}{[M]} \tag{3.4}$$

By combining the vector U with the vector V, we obtain

$$Z = \begin{bmatrix} u_1 \\ u_2 \\ \vdots \\ u_{dof} \\ v_1 \\ v_2 \\ \vdots \\ v_{dof} \end{bmatrix} = \begin{bmatrix} U \\ V \end{bmatrix} \tag{3.5}$$

Thus, the system 3.1 can be written as

$$\dot{Z} = F(Z) = \begin{bmatrix} V \\ f(U) \end{bmatrix} \tag{3.6}$$

This equation can be solved, as mentioned earlier, using a solver implemented in MatLab and optimized for this purpose, called *ode15s*. During this analysis, the vector $F(t)$ is constructed as follows:

$$F(t) = \begin{bmatrix} 0_1 \\ 0_2 \\ \vdots \\ 0_{n-1} \\ F_n \\ 0_{n+1} \\ \vdots \\ 0_{dof} \end{bmatrix} \tag{3.7}$$

In this way, the force is applied at a single degree of freedom in the system, corresponding to the n-th degree of freedom, which is located at the center of the face opposite the clamped face. To verify that the model developed in MatLab is correct, a preliminary static analysis is performed, thus solving

$$[K]\{U\} = \{F\} \tag{3.8}$$

where F is constant and has a chosen value. The result of this simulation gives the unknown vector of translations and rotations of the nodes. This vector is

then used as the initial condition to solve the system 3.6, with the same force $F(t)$ value chosen in the previous simulation. In this way, it is expected that the block, subjected to a force corresponding to a displacement field given as the initial condition, will not undergo any changes over time, and thus the vector U will remain unchanged. This allows for a simple verification of the MatLab script used.

3.2.3 Newmark's method

The system of equations 3.1 could rigorously be solved by applying the Newmark method [34]. This is a direct integration method that discretizes a continuous problem. Given the initial conditions, the goal is to satisfy equation 3.1 at each discrete point in time. Being a direct method, it assumes a specific variation of displacements, velocities, and accelerations within each time interval considered, where the equilibrium equation 3.1 is satisfied at each time step. In particular, this method leverages the mean value theorem and, combined with a standard Taylor's series, approximates the displacement and velocity at the next time instant, t_{n+1}. Applying the mean value theorem, equation 3.1 can be rewritten to derive an expression for the second derivative [35]:

$$\ddot{u}_{n+1} = M^{-1} \left(f(u_{n+1}) - C\dot{u}_{n+1} - Ku_{n+1} \right) \tag{3.9}$$

This equation is solved iteratively, updating u_{n+1} and $\dot{u}_{n+1}$ using the formulas derived earlier from Taylor's series expansion. The method introduces the parameters β and γ. It has been shown that the method is unconditionally stable for $\gamma = \frac{1}{2}$ and $\beta = \frac{1}{4}$ [36], and under these conditions, it is referred to as the average acceleration method.

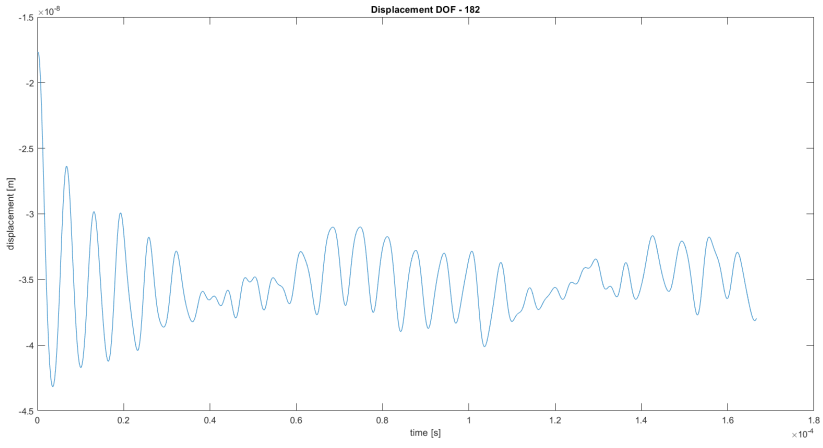

Figure 3.4: Displacement DOF - 182 - system not in equilibrium

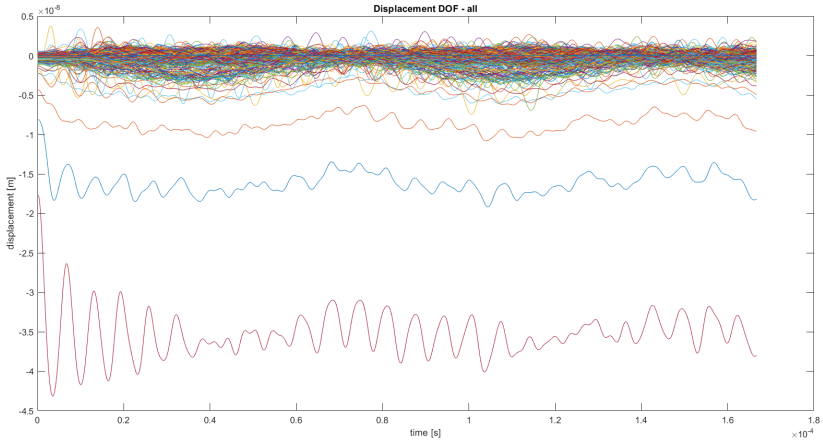

Figure 3.5: Displacement DOF - All - system not in equilibrium

In figures 3.4 and 3.5, the behavior of the DOFs is shown when subjected to a force such that the initial displacement condition is not satisfied. When a force that does not match the equilibrium condition is applied to a system, the system will experience a displacement from its initial state. This causes the system to start vibrating as it attempts to restore equilibrium. The imbalance between the applied force and the internal forces leads to oscillations, as the system continually reacts to the disturbance. Over time, depending on the system's properties, these vibrations may either stabilize, reaching a new equilibrium, or continue oscillating indefinitely. In some cases, the system may gradually lose energy, damping the oscillations, while in other cases, the system may exhibit more complex dynamic behavior.

3.3 Physical considerations

The analysis is conducted using *ode15s*, as this is crucial for connecting the simulation presented in 2.

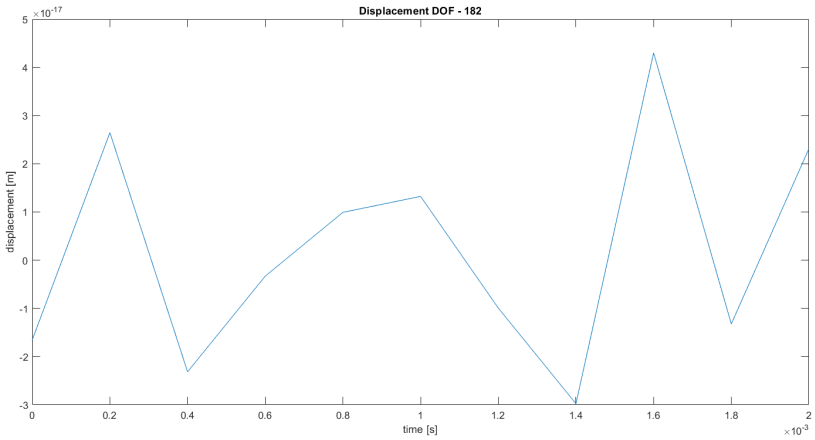

Figure 3.6: Displacement DOF - 182 - system in equilibrium

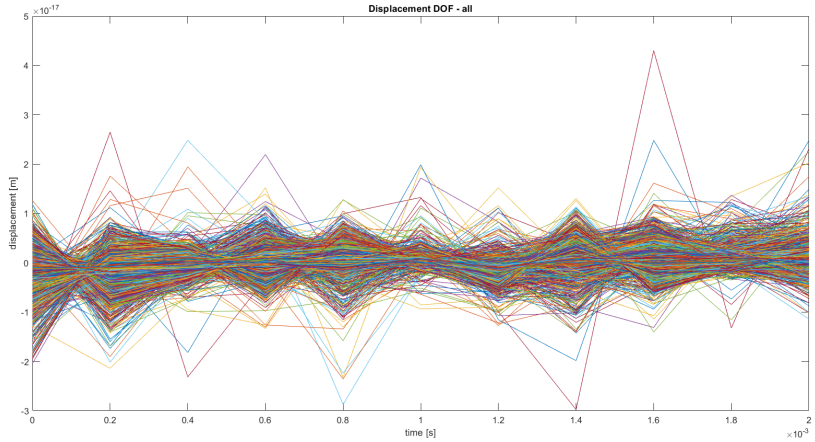

Figure 3.7: Displacement DOF - All - system in equilibrium

Figures 3.6 and 3.7 show the displacement trend of the degrees of freedom of the FEM block, imposing as the initial condition that derived from the analysis in 3.8 and applying a load equal to F. Therefore, it is expected that the system remains in equilibrium under the action of the load F, and this is confirmed by the MatLab code.

Chapter 4

The coupling between DEM and FEM

This chapter presents the mechanism by which the DEM and FEM simulations are coupled.

4.0.1 Implementation

To solve the system of equations governing the system consisting of N spheres, which make up the granular crystal, and the metallic block, it is necessary to solve equations 2.1 and 3.1 simultaneously. To do this, one can construct a vector containing the displacements of each FEM node and each particle of the granular crystal:

$$U = \begin{bmatrix} u_1 \\ u_2 \\ \vdots \\ u_N \\ u_{N+1} \\ \vdots \\ u_{N+dof} \end{bmatrix} \tag{4.1}$$

and a vector containing the time derivative of U:

$$\dot{U} = V \begin{bmatrix} v_1 \\ v_2 \\ \vdots \\ v_N \\ v_{N+1} \\ \vdots \\ v_{N+dof} \end{bmatrix} \tag{4.2}$$

Define a vector consisting of U and V:

$$Z = \begin{bmatrix} u_1 \\ u_2 \\ \vdots \\ u_N \\ u_{N+1} \\ \vdots \\ u_{N+dof} \\ v_1 \\ v_2 \\ \vdots \\ v_N \\ v_{N+1} \\ \vdots \\ v_{N+dof} \end{bmatrix} \tag{4.3}$$

In this way, the system 2.1 + 3.1

$$\begin{cases} m\ddot{u}_n = A_n[u_{n-1} - u_n]_+^{3/2} - A_{n+1}[u_n - u_{n+1}]_+^{3/2} + mg, \quad n \in \{1, \dots, N\} \\ \\ [M]\{\ddot{U}\} + [C]\{\dot{U}\} + [K]\{U\} = \{F(t)\}, \quad n \in \{N+1, \dots, N+dof\} \end{cases} \tag{4.4}$$

can be rewritten as

$$\dot{Z} = F(Z) = \begin{bmatrix} V \\ f(U) \end{bmatrix} \tag{4.5}$$

Being a system of differential equations, initial conditions U_0 and V_0 must be provided. Specifically, V_0 will be a vector containing $N + dof - 1$ zero elements and a single non-zero element (the first one) representing the velocity of the first particle, which acts as the striker for the system. Instead of using a striker and

thus assigning a non-zero initial velocity to the first particle, one could consider assigning an initial displacement to the first particle, which corresponds to a certain initial Hertzian force that sets the particle system in motion. As for the vector U_0, it will be constructed such that the part of the block has displacement values corresponding to the static force applied to the last particle. Therefore, as the first step, the system of equations 3.8 is solved, and the obtained displacement field is used as the initial condition. By doing this, the displacement corresponding to the contact node between the block and the last sphere must be added to each sphere so that, initially, spheres and the block remain in contact and there are no gaps. Thus,

$$U_{0_{1\ldots N}} = U_n \tag{4.6}$$

where n is the degree of freedom related to the contact point between the block and the granular crystal. Furthermore, since a force is applied to the last sphere, in order to observe the effects of introducing friction into the system, it is necessary to first include this force in the equation for the last particle. To ensure that the simulation proceeds correctly, it is important to consider an initial penetration between the sphere under this force and the block. This penetration, through a Hertzian force, will balance the force applied to the last particle. This initial penetration is given by

$$U_{0_N} = \Big(\frac{Load}{A_{N+1}}\Big)^{\frac{2}{3}} \tag{4.7}$$

This value is added to the other spheres to maintain initial contact. After the simulation, some checks are performed to confirm the validity of the results. In particular, the stiffness of the FEM node and the last particle is calculated:

$$k_{fem} = \frac{Load}{u0_{N+n}} = 10343\frac{N}{\mu m} \tag{4.8}$$

$$k_N = \frac{Load}{u0_N - u0_{N+n}} = 8.3289\frac{N}{\mu m} \tag{4.9}$$

Thus, we expect a displacement that is $\frac{10343}{8.3289} = 125$ times greater for the last sphere compared to the FEM node, which can be observed in the following figures:

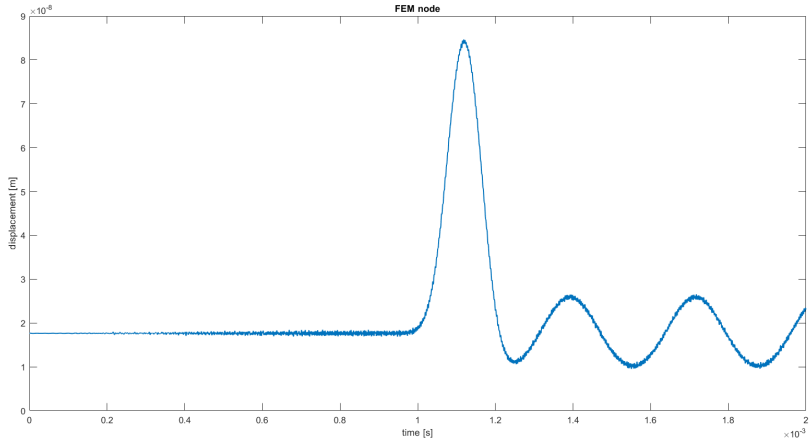

Figure 4.1: FEM node displacement vs time

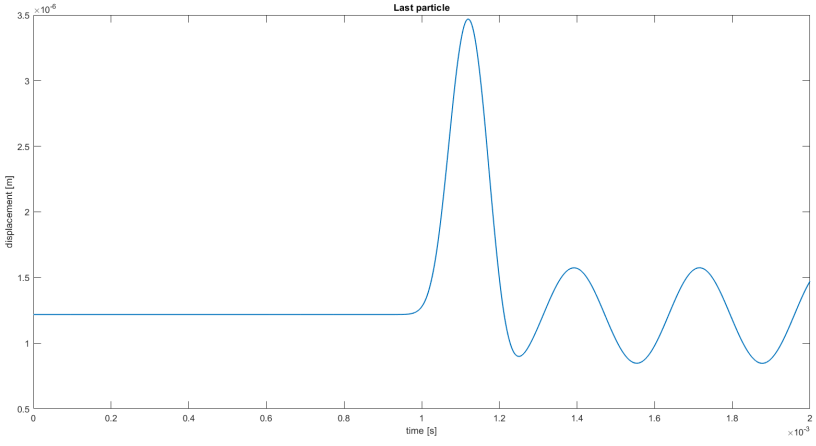

Figure 4.2: Last particle displacement vs time

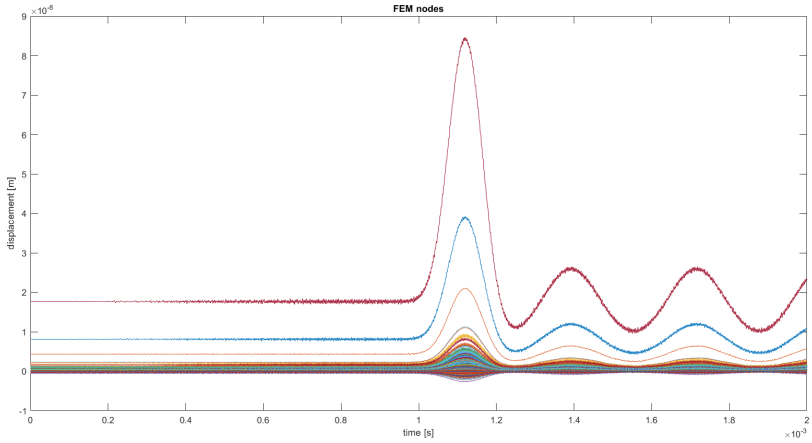

Figure 4.3: FEM nodes displacement vs time

Figure 4.4 shows, similarly to figure 2.2, the displacement and velocity trends of the N spherical particles. It can be seen that, unlike figure 2.2, by applying a preload to the last particle, it will experience an oscillatory motion back and forth along the horizontal axis of the reference system.

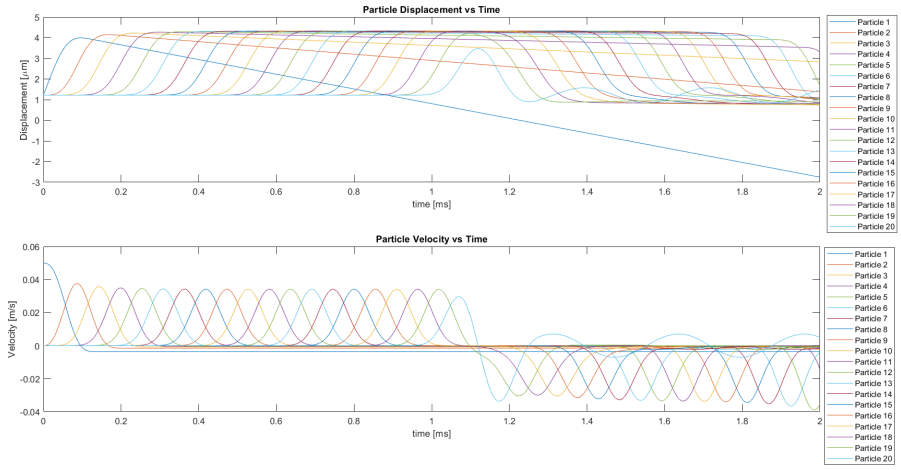

Figure 4.4: Displacement and velocity trend

Another check that can be done is to evaluate the Hertzian force between the last sphere and the FEM node, which should equal the preload force applied to the last sphere. We indeed get that

$$F_{Hertz} = A_{N+1}(u_{0_N} - u_{0_{N+n}})^{\frac{3}{2}} = F_{preload} \tag{4.10}$$

4.1 FEM Mesh Selection

The block mesh performed using Abaqus is a very important procedure as described by [37]. To accurately analyze the problem, it is necessary to choose a reference size for the FEM elements. Each element is chosen to be of a size such that its area is smaller than the contact area between the sphere and the block. To calculate this value, it is first necessary to evaluate the equivalent Young's modulus of elasticity [4]:

$$\frac{1}{E^*} = \frac{1-\nu_1^2}{E_1} + \frac{1-\nu_2^2}{E_2} \tag{4.11}$$

where 1 and 2 refer to the respective body 1 and body 2 in question. The contact area between the two bodies is given by [38]:

$$a = \Big(\frac{3NR}{4E^*}\Big)^{\frac{1}{3}} \tag{4.12}$$

where R is the radius of the sphere and N is the normal load.

4.2 Representation of the Granular Crystal - FEM Block System

Looking at what physically happens in the system, it is noticed that the solitary wave, formed from the initial impact at velocity v_0 of the first spherical particle against the second, propagates along the granular chain through the Hertzian penetration mechanism between spheres. Once the solitary wave reaches the FEM block, it reacts by deforming at the node that connects it to the granular crystal, and consequently to the nearby nodes, following the reference equation of motion 3.1.

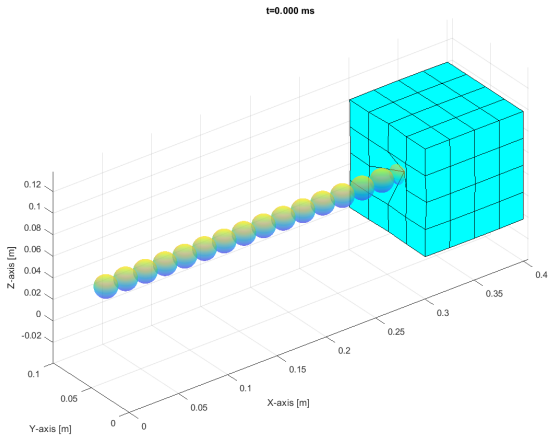

Figure 4.5: System at the initial time

In figure 4.5, we can finally observe the schematic of the system. It can be seen that, at the initial instant, the last sphere is already in penetration with the FEM block. This is due to the reasons mentioned in 4.0.1.

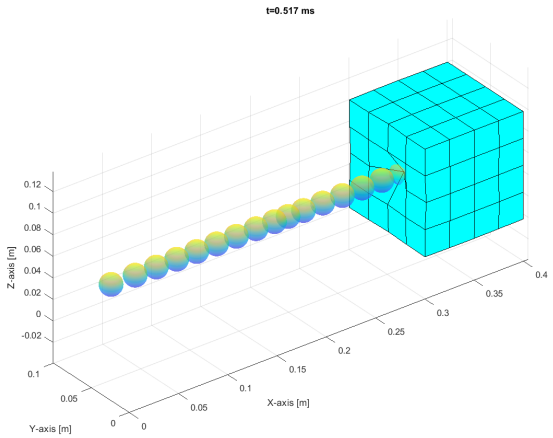

Figure 4.6: System at a generic time instant

Taking a time step subsequent to the initial one, it can be observed (see figure 4.6) how the solitary wave is propagating, as the penetration phase of one sphere into another is visible, followed by a depenetration phase between the two, allowing space for a new penetration with the next sphere. In this way, the solitary wave propagates.

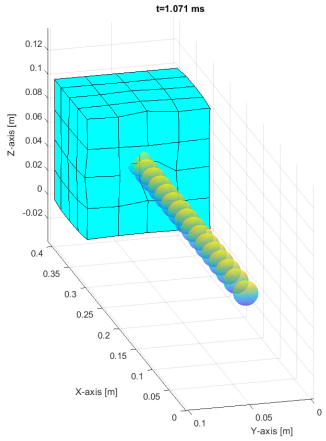

Figure 4.7: System at the instant when the last sphere penetrates into the FEM block

At this time step, the penetration of the last sphere into the FEM block is observed. Through a multiplicative factor, it is possible to see this penetration and the subsequent relaxation due to the inversion of the motion of the last particle. From the displacement-time graphs in figure 4.4, it is noted that this particle begins to oscillate once the wave has passed through it for the second time. This could experimentally cause stability issues in the test system. To try to attenuate this oscillation, one could consider applying a preload to the first particle in the chain (chosen for simplicity, but any other sphere could theoretically be used), in a similar manner to what was done with the last particle. This leads to a reduction in the oscillation, which can be qualitatively observed in figure 4.8

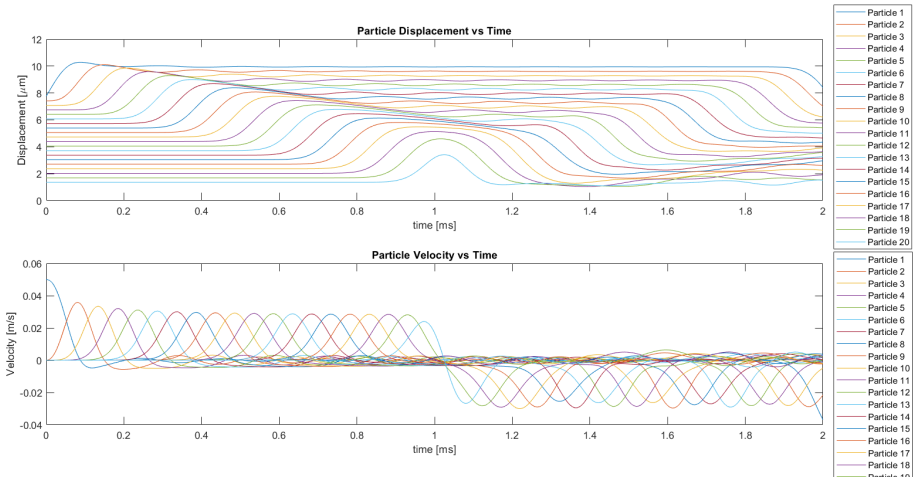

Figure 4.8: Displacement and velocity trend - preload applied to the first particle

Chapter 5

Friction

In this chapter, the procedure for considering friction in the model is presented. In particular, friction is introduced between the last sphere of the granular crystal and the metal block in order to plot the hysteresis curve.

5.1 Jenkins Element

In order to plot the hysteresis cycle, it is necessary to choose a contact model and thus an element to simulate the behavior of the component subjected to friction. In particular, a Jenkins element [39] is chosen, which is based on Coulomb's law as shown in 5.1.

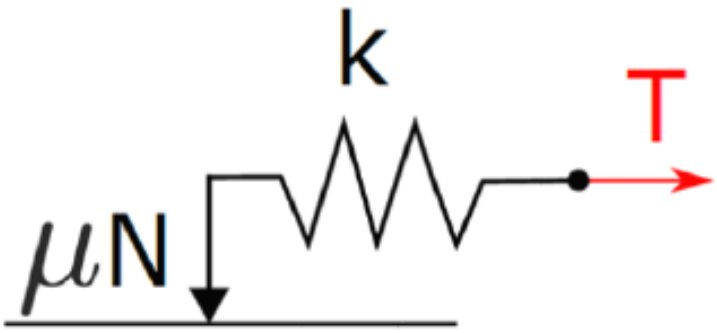

Figure 5.1: Jenkins element model

The peculiarity of this model is that it describes the gross slip regime of the hysteresis loop without considering the microslip regime (i.e., the regime where a

portion of the contact surface slips while the remaining part of the surface is stuck). This element, also known as the friction slider, is composed of several components:

- Elastic spring
- Coulomb element

In particular, the elastic spring is in series with the Coulomb element, as shown in 5.1. The elastic spring, which is essentially a tangential contact stiffness k_t, relates the force linearly to the displacement:

$$T = k_t \cdot x \tag{5.1}$$

While the Coulomb element follows the Amontons-Coulomb law:

$$T = \mu \cdot N \tag{5.2}$$

where N is the normal force applied to the contact surface. Thanks to the use of a Jenkins element, it is possible to generate a hysteresis loop (such as the one in figure 5.2), but without the ability to describe the microslip regime. However, the potential of this contact model lies in the fact that by modeling the contact surface with enough FE nodes coupled by different Jenkins elements, some nodes will be in the slip regime and others in the stick regime, thus representing the microslip regime.

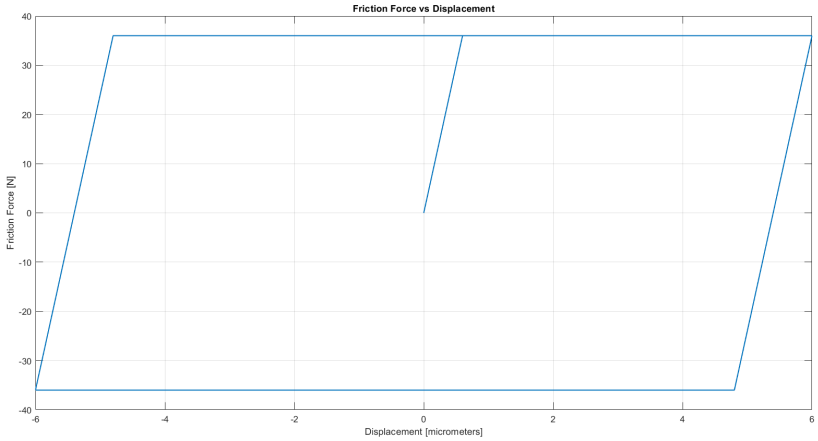

Figure 5.2: Hysteresis loop

To solve the system formed by equations 5.1 and 5.2, a numerical method must be implemented, which is described in section 5.2.

5.2 Numerical Method

The numerical method to solve a hysteresis loop problem consists of several phases:

- Normal force acquisition: the normal force exchanged between the granular crystal and the metal block.
- Definition of sinusoidal horizontal displacement: the displacement imposed on the block.
- Prediction of the motion regime: a certain condition between stick and slip is predicted (in our case, it was chosen to predict being in the stick phase by evaluating the value of the tangential contact force using 5.1).
- Verification of the prediction: if the condition is verified, the process continues; otherwise, the tangential contact force is reevaluated using 5.2.

5.3 Discussion

The hysteresis graph obtained is shown in figure 5.3.

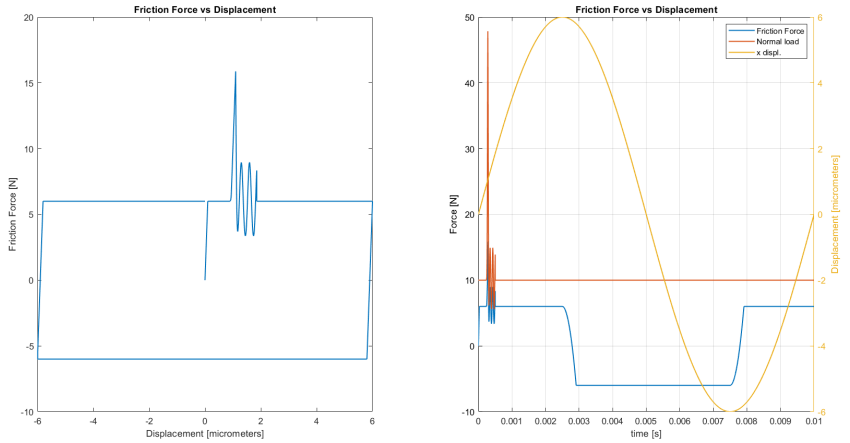

Figure 5.3: Hysteresis loop

It can be observed that, unlike the graph in figure 1.1, which presents the shape of a parallelogram due to the two stick and slip regimes, there is an "oscillation" during the slip phase. This is due to the solitary wave impacting the FEM block. Specifically, the solitary wave, when it hits and passes through the FEM block, generates a $\Delta NormalLoad$, which manifests physically as seen in figure 5.3. The increase in friction force is due to the fact that, following the increase in normal

force, the Coulomb limit μN increases, leading to a sticking phase. It is also interesting to observe the right side of figure 5.3, as it shows the behavior of the normal load and how it changes after about 0.0005 seconds. This is the time it takes for the wave to reach the FEM block. For this analysis, the friction mechanism was considered decoupled from the transfer of normal load between the two elements considered.

Chapter 6

Conclusion and future developments

6.1 Conclusion

In this Master Thesis, a MATLAB code was developed to simulate solitary wave propagation within a granular crystal (modeled using DEM) and its interaction with a metallic block (modeled using FEM). Particular attention was given to the friction mechanism and how it can be evaluated through variations in a hysteresis loop. The key findings include:

- **Wave propagation**: The solitary wave within the granular crystal follows Hertzian contact laws, while its interaction with the FEM block induces localized deformations and oscillatory responses.

- **Contact mechanics**: The choice of FEM mesh size, based on the contact area, enables an accurate representation of stresses and displacements at the sphere-block interface.

- **Friction modeling**: By implementing the Jenkins element, which allows the reproduction of a hysteresis loop, it is possible to evaluate the energy dissipated during the process.

This Master Thesis contributes to a broader understanding of coupled granular-FEM systems, with potential applications in advanced materials design, energy dissipation systems, and wave propagation studies. Therefore, it can be regarded as an initial step toward future investigations in this field, which remains rich with opportunities for discovery.

6.2 Future Developments

The topic addressed in this Master Thesis remains an area of ongoing research among leading research groups worldwide. To summarize, some potential areas for future developments include:

- **Considering Macroslip Regimes**: Introducing a more refined contact model that can capture this regime within the hysteresis loop. This could be achieved by implementing a distributed Jenkins element across multiple FEM elements or by employing alternative contact models, such as the Mindlin model.
- **Incorporation of Nonlinearities**: Enhancing the FEM block model by including nonlinearities to allow for plastic or viscoelastic deformations.
- **Multiphysics Coupling**: Introducing thermal and electromagnetic effects, which could alter the mechanical properties of both the granular crystal and the FEM block.
- **Experimental Validation**: This component is fundamental for validating a numerical code. In this regard, Dr. Fantetti's research group is currently working on conducting laboratory experiments for the system simulated so far.

Appendix A

Matrix Extraction from Abaqus

A.1 Mass and Stiffness

The procedure for obtaining the mass matrix and the stiffness matrix involves performing a frequency analysis of the structure under consideration. To be as comprehensive as possible, the steps to follow are listed below:

1. Geometry Creation: This is done using the part module.
2. Material Definition: The material is defined using the property module by specifying the values for density, Poisson's ratio, and elastic modulus.
3. Section Creation and Assignment: The section is assigned to the part created earlier through the appropriate command.
4. Assembly: The instance is created in the assembly module.
5. Step: A step is created using "Linear perturbation → frequency," requesting 10 eigenvalues.
6. Boundary Conditions: Boundary conditions are applied in the previously created step.
7. Mesh: The part is meshed.
8. Job Creation: A job is created, and the input file is written.
9. Input File Modification: The .inp file is modified by adding the following code string between the material definition and the step:

```
*STEP, NAME=export matrix
*MATRIX GENERATE, STIFFNESS, MASS
*MATRIX OUTPUT, STIFFNESS, MASS, FORMAT=COORDINATE
*END STEP
```

10. Run the Job: The modified .inp file is run through PowerShell by typing: `abaqus j = job - 1 int` where job-1 is the name of the .inp file, for example. **Note:** The .inp file must be in the same directory.

The matrices are now available. To be used, they must be converted into .txt files so that they can be read in MATLAB using the *read matrix* command.

A.2 Force

In order to perform the static and dynamic analysis of the FEM block, it is necessary to know on which DOF the force will be applied. This DOF corresponds to the degree of freedom in the direction equal to the direction of the force applied to the central node of the face opposite to the fixed face. The steps to obtain this matrix involve a static analysis and are listed below:

1. Geometry Creation: This is done using the part module.
2. Material Definition: The material is defined using the property module by specifying the values for density, Poisson's ratio, and elastic modulus.
3. Section Creation and Assignment: The section is assigned to the part created earlier through the appropriate command.
4. Assembly: The instance is created in the assembly module.
5. Step: A step is created using "General → static, general"
6. Boundary conditions and load: The boundary conditions and the load applied at the node of interest are defined.
7. Mesh: The part is meshed.
8. Job Creation: A job is created, and the input file is written.
9. Input File Modification: The .inp file is modified by adding the following code string at the end of the code:
```
*STEP
*MATRIX GENERATE, STIFFNESS, LOAD
*MATRIX OUTPUT, STIFFNESS, LOAD, FORMAT=COORDINATE
```

```
**
** LOADS
**
...
**
*END STEP
```

10. Modification of the Loads Section: Instead of ..., the corresponding load already present in the input file must be inserted by copying and pasting it.

The force matrix consists of a number corresponding to the DOF on which the force is applied, and the force itself. Simply put, the DOF is used in MATLAB to perform the static analysis prior to the simulation with granular crystal in order to apply the correct initial conditions.

Bibliography

[1] Nan Gao, Tianxue Ma, Yize Wang, Weijian Zhou, Yue-Sheng Wang, and Weiqiu Chen. «A brief review of solitary waves in nonlinear metamaterials». In: *Mechanics Research Communications* 137 (2024), p. 104260. ISSN: 0093-6413. DOI: https://doi.org/10.1016/j.mechrescom.2024.104260. URL: https://www.sciencedirect.com/science/article/pii/S0093641324000181 (cit. on pp. 1, 3).

[2] V. Nesterenko. «Propagation of nonlinear compression pulses in granular media». In: *Journal of Applied Mechanics and Technical Physics - J APPL MECH TECH PHYS* 24 (Nov. 1983), pp. 733–743. DOI: 10.1007/BF00905892 (cit. on p. 2).

[3] A. Lazaridi and V. Nesterenko. «Observation of a new type of solitary waves in one-dimensional granular medium». In: *Journal of Applied Mechanics and Technical Physics - J APPL MECH TECH PHYS* 26 (May 1985), pp. 405–408. DOI: 10.1007/BF00910379 (cit. on p. 2).

[4] K. L. Johnson. «Normal contact of elastic solids – Hertz theory». In: *Contact Mechanics*. Cambridge University Press, 1985, pp. 84–106 (cit. on pp. 2, 34).

[5] Vitali Nesterenko. *Dynamics of heterogeneous materials*. Springer Science & Business Media, 2013 (cit. on p. 3).

[6] Jinkyu Yang, Devvrath Khatri, Paul Anzel, and Chiara Daraio. «Interaction of highly nonlinear solitary waves with thin plates». In: *International Journal of Solids and Structures* 49.13 (2012), pp. 1463–1471. ISSN: 0020-7683. DOI: https://doi.org/10.1016/j.ijsolstr.2012.02.013. URL: https://www.sciencedirect.com/science/article/pii/S0020768312000534 (cit. on pp. 3, 9, 17, 18).

[7] R. Carretero-González, D. Khatri, Mason A. Porter, P. G. Kevrekidis, and C. Daraio. «Dissipative Solitary Waves in Granular Crystals». In: *Phys. Rev. Lett.* 102 (2 Jan. 2009), p. 024102. DOI: 10.1103/PhysRevLett.102.024102. URL: https://link.aps.org/doi/10.1103/PhysRevLett.102.024102 (cit. on pp. 3, 19).

[8] Hoda Jalali and Piervincenzo Rizzo. «Numerical investigation of the interaction of highly nonlinear solitary waves with corroded steel plates». In: *International Journal of Mechanical Sciences* 208 (2021), p. 106676. ISSN: 0020-7403. DOI: https://doi.org/10.1016/j.ijmecsci.2021.106676. URL: https://www.sciencedirect.com/science/article/pii/S0020740321004070 (cit. on p. 4).

[9] Francisco Santibanez, Romina Munoz, Aude Caussarieu, Stéphane Job, and Francisco Melo. «Experimental evidence of solitary wave interaction in Hertzian chains». In: *Physical Review E* 84.2 (Aug. 2011). ISSN: 1550-2376. DOI: 10.1103/physreve.84.026604. URL: http://dx.doi.org/10.1103/PhysRevE.84.026604 (cit. on p. 4).

[10] Alfredo Fantetti, Daniele Botto, Stefano Zucca, and Christoph Schwingshackl. «Guidelines to use input contact parameters for nonlinear dynamic analysis of jointed structures: Results of a round robin test». In: *Tribology International* 191 (2024), p. 109158. ISSN: 0301-679X. DOI: https://doi.org/10.1016/j.triboint.2023.109158. URL: https://www.sciencedirect.com/science/article/pii/S0301679X23009490 (cit. on pp. 4, 5).

[11] Peter J. Blau. «Friction, History of Research». In: *Encyclopedia of Tribology*. Ed. by Q. Jane Wang and Yip-Wah Chung. Boston, MA: Springer US, 2013, pp. 1384–1386. ISBN: 978-0-387-92897-5. DOI: 10.1007/978-0-387-92897-5_189. URL: https://doi.org/10.1007/978-0-387-92897-5_189 (cit. on p. 6).

[12] Xuanming Liang, XING Z, Li Leitao, Yuan Weike, and Gangfeng Wang. «An experimental study on the relation between friction force and real contact area». In: *Scientific Reports* 11 (Oct. 2021), p. 20366. DOI: 10.1038/s41598-021-99909-2 (cit. on p. 6).

[13] Frank Philip Bowden and David Tabor. «The Area of Contact between Stationary and between Moving Surfaces». In: *Proceedings of The Royal Society A: Mathematical, Physical and Engineering Sciences* 169 (1939), pp. 391–413. URL: https://api.semanticscholar.org/CorpusID:130092819 (cit. on p. 6).

[14] H. G. Howell. «The Laws of Friction». In: *Nature* 171 (1953), pp. 220–220. URL: https://api.semanticscholar.org/CorpusID:4208568 (cit. on p. 6).

[15] S. Bograd, P. Reuss, A. Schmidt, L. Gaul, and M. Mayer. «Modeling the dynamics of mechanical joints». In: *Mechanical Systems and Signal Processing* 25.8 (2011), pp. 2801–2826. ISSN: 0888-3270. DOI: https://doi.org/10.1016/j.ymssp.2011.01.010. URL: https://www.sciencedirect.com/science/article/pii/S0888327011000203 (cit. on p. 6).

[16] Ettore Pennestri, Valerio Rossi, Pietro Salvini, and Pier Paolo Valentini. «Review and comparison of dry friction force models». In: *Nonlinear Dynamics* 83 (Mar. 2016). DOI: 10.1007/s11071-015-2485-3 (cit. on p. 7).

[17] SILVIA CAPRINO, GUIDO CAVALLARO, and CARLO MARCHIORO. «ON A MICROSCOPIC MODEL OF VISCOUS FRICTION». In: *Mathematical Models and Methods in Applied Sciences* 17.09 (2007), pp. 1369–1403. DOI: 10.1142/S0218202507002315. eprint: https://doi.org/10.1142/S0218202507002315. URL: https://doi.org/10.1142/S0218202507002315 (cit. on p. 7).

[18] Hamed Kashani. «PARAMETRIC STUDY OF NONLINEAR BEHAVIOR OF JENKINS ELEMENT USING HARMONIC BALANCE METHOD». In: 2013. URL: https://api.semanticscholar.org/CorpusID:214791880 (cit. on p. 7).

[19] Philip DAHL. «Solid friction damping of spacecraft oscillations». In: *Guidance and Control Conference*. 1975, p. 1104 (cit. on p. 7).

[20] Leonid Freidovich, Anders Robertsson, Anton Shiriaev, and Rolf Johansson. «LuGre-model-based friction compensation». In: *IEEE Transactions on Control Systems Technology* 18.1 (2009), pp. 194–200 (cit. on p. 7).

[21] Xiaobin Lu, M. Khonsari, and Edwin Gelinck. «The Stribeck Curve: Experimental Results and Theoretical Prediction». In: *Journal of Tribology-transactions of The Asme - J TRIBOL-TRANS ASME* 128 (Oct. 2006). DOI: 10.1115/1.2345406 (cit. on p. 7).

[22] Vincent Lampaert, Jan Swevers, and Farid Al-Bender. «Modification of the Leuven integrated friction model structure». In: *Automatic Control, IEEE Transactions on* 47 (May 2002), pp. 683–687. DOI: 10.1109/9.995050 (cit. on p. 7).

[23] Georg Masing. «Zur Heyn'schen Theorie der Verfestigung der Metalle durch verborgen elastische Spannungen». In: *Wissenschaftliche Veröffentlichungen aus dem Siemens-Konzern: III. Band*. Ed. by Carl Dietrich Harries. Berlin, Heidelberg: Springer Berlin Heidelberg, 1923, pp. 231–239. ISBN: 978-3-642-99663-4. DOI: 10.1007/978-3-642-99663-4_17. URL: https://doi.org/10.1007/978-3-642-99663-4_17 (cit. on p. 7).

[24] Dongwu Li, Daniele Botto, Chao Xu, and Muzio Gola. «A new approach for the determination of the Iwan density function in modeling friction contact». In: *International Journal of Mechanical Sciences* 180 (2020), p. 105671. ISSN: 0020-7403. DOI: https://doi.org/10.1016/j.ijmecsci.2020.105671. URL: https://www.sciencedirect.com/science/article/pii/S0020740319348258 (cit. on p. 7).

[25] Zakieh Avazzadeh, Omid Nikan, and José A Tenreiro Machado. «Solitary wave solutions of the generalized Rosenau-KdV-RLW equation». In: *Mathematics* 8.9 (2020), p. 1601 (cit. on p. 10).

[26] Chongan Wang, Qifan Zhang, and Alexander F. Vakakis. «Wave transmission in 2D nonlinear granular-solid interfaces, including rotational and frictional effects». English (US). In: *Granular Matter* 23.2 (May 2021). Publisher Copyright: © 2021, The Author(s), under exclusive licence to Springer-Verlag GmbH, DE part of Springer Nature. ISSN: 1434-5021. DOI: 10.1007/s10035-021-01093-7 (cit. on p. 13).

[27] Eunho Kim, Francesco Restuccia, Jinkyu Yang, and Chiara Daraio. «Solitary wave-based delamination detection in composite plates using a combined granular crystal sensor and actuator». In: *Smart Materials and Structures* 24.12 (2015), p. 125004 (cit. on p. 17).

[28] Clarence Zener. «The Intrinsic Inelasticity of Large Plates». In: *Phys. Rev.* 59 (8 Apr. 1941), pp. 669–673. DOI: 10.1103/PhysRev.59.669. URL: https://link.aps.org/doi/10.1103/PhysRev.59.669 (cit. on p. 18).

[29] J Tillett. «A Study of the Impact of Spheres on Plates». In: *Proceedings of the Physical Society. Section B* 67 (Dec. 2002), p. 677. DOI: 10.1088/0370-1301/67/9/304 (cit. on p. 18).

[30] Stéphane Job, Francisco Melo, Adam Sokolow, and Surajit Sen. «How Hertzian Solitary Waves Interact with Boundaries in a 1D Granular Medium». In: *Phys. Rev. Lett.* 94 (17 May 2005), p. 178002. DOI: 10.1103/PhysRevLett.94.178002. URL: https://link.aps.org/doi/10.1103/PhysRevLett.94.178002 (cit. on p. 19).

[31] Michael Smith. *ABAQUS/Standard User's Manual, Version 6.9*. English. United States: Dassault Systèmes Simulia Corp, 2009 (cit. on p. 21).

[32] P. Rugarli. *Calcolo strutturale con gli elementi finiti. Una spiegazione di base del metodo degli elementi finiti applicato all'ingegneria strutturale. Con CD-ROM*. Quaderni per la progettazione. EPC Libri, 2004. ISBN: 9788881842957. URL: https://books.google.it/books?id=jqTTPAAACAAJ (cit. on p. 22).

[33] Lawrence F. Shampine and Mark W. Reichelt. «The MATLAB ODE Suite». In: *SIAM Journal on Scientific Computing* 18.1 (1997), pp. 1–22. DOI: 10.1137/S1064827594276424. eprint: https://doi.org/10.1137/S1064827594276424. URL: https://doi.org/10.1137/S1064827594276424 (cit. on p. 24).

[34] H Hashamdar, Z Ibrahim, and M Jameel. «Finite element analysis of nonlinear structures with Newmark method». In: *International Journal of the Physical Sciences* 6.6 (2011), pp. 1395–1403 (cit. on p. 26).

[35] George Lindfield and John Penny. «Chapter 5 - Solution of Differential Equations». In: *Numerical Methods (Fourth Edition)*. Ed. by George Lindfield and John Penny. Fourth Edition. Academic Press, 2019, pp. 239–299. ISBN: 978-0-12-812256-3. DOI: https://doi.org/10.1016/B978-0-12-812256-3.00014-2. URL: https://www.sciencedirect.com/science/article/pii/B9780128122563000142 (cit. on p. 26).

[36] Henri P. Gavin and Henri P. Gavin. «Numerical Integration in Structural Dynamics». In: 2016. URL: https://api.semanticscholar.org/CorpusID:40330486 (cit. on p. 26).

[37] K. Ho-Le. «Finite element mesh generation methods: a review and classification». In: *Computer-Aided Design* 20.1 (1988), pp. 27–38. ISSN: 0010-4485. DOI: https://doi.org/10.1016/0010-4485(88)90138-8. URL: https://www.sciencedirect.com/science/article/pii/0010448588901388 (cit. on p. 34).

[38] VL Popov. *Contact Mechanics and Friction: Physical Principles and Applications*. 2010 (cit. on p. 34).

[39] Yekai Sun, Jie Yuan, Luca Pesaresi, and Loïc Salles. «Nonlinear Vibrational Analysis for Integrally Bladed Disk Using Frictional Ring Damper». In: *Journal of Physics: Conference Series* 1106.1 (Oct. 2018), p. 012026. DOI: 10.1088/1742-6596/1106/1/012026. URL: https://dx.doi.org/10.1088/1742-6596/1106/1/012026 (cit. on p. 38).